**Title**: Fitness-for-Purpose Assessment of Cracked Offshore Wind Turbine Monopile

Fajuyigbe, A.[a1], Brennan, F.[a]

[a] *Department of Naval Architecture, Ocean and Marine Engineering, University of Strathclyde, G4 0LZ, Glasgow, UK*

## ABSTRACT

In this paper, the procedure for flaw acceptability assessment is examined through a case study of a semi-elliptical surface crack in an offshore monopile as it grows till it forms a through thickness crack. Using the procedure prescribed in an industrial standard (BS 7910), the fracture ratio, $K_r$ is shown to increase monotonically with increasing crack depth. The load ratio, $L_r$, is initially insensitive to the crack depth. However, there is a rapid increase in $L_r$ when the crack depth to thickness ratio exceeds 80%. $L_r$ values obtained from detailed 3D FE limit analysis using elastic-perfectly-plastic material behaviour do not exhibit the asymptotic behaviour predicted by BS 7910 as the flaw transitions from deep crack to through-thickness crack. Furthermore, $K_r$ predicted by BS 7910 is shown to be an over-estimation for the typical dimensions of offshore monopiles. The findings suggest that a structure with a deep flaw may be identified as unacceptable based on BS 7910 when it may still possess a non-trivial amount of structural residual life. This is a concern for monopiles where crack growth as a large flaw forms a significant part of the total life.

## KEYWORDS

Failure Assessment Diagram, Fracture Ratio, Load Ratio, Stress Intensity Factor, Reference Stress, Limit Load, Monopile

## HIGHLIGHTS

- Evaluation of the acceptability of a known flaw in an offshore wind turbine monopile.
- Examination of crack behavior at transition of surface crack to through thickness crack.
- Description of limit load finite element analysis for offshore wind turbine monopile.
- Comparison of BS 7910 flaw acceptability procedure to finite element analysis results.

[1*] = corresponding author details: Ayodele.fajuyigbe@strath.ac.uk

# 1 INTRODUCTION

In 2016, 12% of the installed wind turbine capacity in Europe was older than 15 years. This share increases to 28% by 2020. These wind turbines will soon reach the end of their designed service life, which is typically 20 years. As a consequence, the wind industry needs to prepare for upcoming challenges, such as maintenance of aging assets, assessment of structural integrity, lifetime extension decision making, and decommissioning of turbines [1].

There is little experience in the re-assessment of wind turbines to quantify remaining useful life. Recommendations from recently published industry standard [2] suggest a two-part process. The first is an analytical part involving damage re-calculation for the wind turbine, considering the site-specific installations and its local conditions. The second is a practical part consisting of assessment through inspection of the wind turbine considering the maintenance/operational history and the turbine type related field experience. As an aged structure is likely to already contain a flaw either due to manufacturing defects or through system loading, it is necessary to assess the fitness for service of a structure known to contain a flaw, that is, ascertain if a known crack is likely to cause of structure to fail under applied load.

Linear-elastic fracture mechanics (LEFM) models are used to characterise crack growth as a function of stress cycles, structural and crack geometry, and material parameters. The models allow the investigation of the second fatigue phase (crack propagation) to ascertain the conditions under which a crack will grow to a point at which further crack growths are unrestricted. There are several industrial standards outlining recommendations for the use of LEFM models in determining the acceptability of flaws in metallic structures such as BS 7910 - Guide to methods for assessing the acceptability of flaws in metallic structures [3] and API 579 – Fitness for Service [4].

This paper examines the approach laid out in BS 7910. BS 7910 was driven by the need of the oil and gas industry in the 1960s and 1970s to provide a technically sound, transparent, accurate, user-friendly and free from commercial bias approach for assessing flaws in welded structures using a fracture mechanics approach rather than rules based on workmanship. A brief history of BS 7910 is provided in [5].

Using an exemplar OWT monopile foundation as a case study, a surface flaw growing under the action fatigue loads is assessed to investigate the failure mode of the structure. The remainder of this paper is organized as follows: Section 2 presents a brief exposition into the primary tool used to assess acceptability of flaw in BS 7910. The parameters of the OWT and the adopted methodology are presented in section 3. The results are discussed in section 4. The conclusions and outlook are presented in section 5.

# 2 FAILURE ASSESSMENT DIAGRAMS

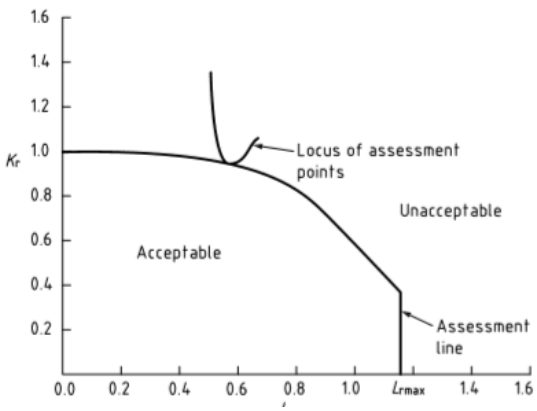


**Figure 2.1 – Failure Assessment Diagram**

For BS 7910, the acceptability of a flaw is based on its position on the failure assessment diagram (FAD). FADs provide a methodology, or framework, for demonstrating the proximity to failure of components containing crack-like defects. The FAD delineates regions of safe operation based on empirical data for different materials. The ordinate plots $K_r$; a measure of the susceptibility of the structure's unstable brittle fracture failure in the presence of a crack calculated using linear elastic fracture mechanics. The abscissa plots $L_r$; a measure of the susceptibility of the structure to plastic collapse as is typical of less brittle or ductile materials where the microstructure allows for deformation/flow of the material. The assessment line is cut-off at the point $L_r = L_{r,max}$ to prevent plastic collapse. For any loading condition, if $K_r$ and $L_r$ fall below the assessment line, the flaw is deemed acceptable.

The generation of the assessment line is heavily dependent on the amount of information available about the material. BS 7910 provides 3 levels of calculation, the so-called options 1 to 3. The complexity of the information required to generate the assessment line increases with the levels, however, the level of conservatism in the analysis decreases.

Option 2 is based on the use of a material-specific stress-strain curve. Option 3 uses numerical analysis to generate a FAD and is not confined to use with materials showing ductile tearing. Option 1 is adopted for this paper. It is a conservative procedure that is relatively simple to employ and does not require detailed stress/strain data for the materials being analysed. It is assumed that the material does not exhibit yield discontinuity in line with recommendations provided in clause 7.1.3.6 of BS 7910. From BS 7910, the governing equations for option 1 FAD line are as follows:

$$f(L_r)\begin{cases}\left(1+\frac{1}{2}L_r^2\right)^{-1/2}\left[0.3+0.7e^{-\mu L_r^6}\right] & L_r \le 1\\ f(1)L_r^{(N-1)(2N)} & 1 < L_r < L_{r,max}\\ 0 & L_r \ge L_{r,max}\end{cases} \tag{1}$$

$$\mu = min\left[0.001\frac{E}{\sigma_Y}, 0.6\right] \qquad N = 0.3\left[1-\frac{\sigma_Y}{\sigma_u}\right]$$

$$L_{r,max} = \frac{\sigma_Y + \sigma_u}{2\sigma_Y}$$

$\sigma_Y$ is the lower of yield or 0.2% proof strength, $\sigma_u$ is the tensile strength and $E$ is the elastic modulus.

## 2.1 Fracture and Load Ratio

For each crack geometry and loading conditions the fracture ratio, $K_r$ ratio is calculated as:

$$K_r = \frac{K_I^p + VK_I^s}{K_{mat}} \tag{2}$$

$K_I^p$ is the stress intensity factor (SIF) at the current crack size due to the primary stresses. Primary stresses are defined as those that can contribute to plastic collapse such as internal pressure and external loads

$K_I^S$ is the stress intensity factor at the current crack size due to secondary stresses. Secondary loads are self-equilibrating loads necessary to satisfy compatibility of the structure such as thermal and residual stresses. Secondary stresses are not considered in this paper.

$K_{mat}$ is the fracture toughness taking account of any ductile tearing following initiation.

$V$ is a function of the primary and secondary loads and accounts for plasticity interaction.

The load ratio, $L_r$ is calculated as:

$$L_r = \frac{\sigma_{ref}}{\sigma_Y} = \frac{P}{P_L}\left(= \frac{applied\ load}{limit\ load}\right) \tag{3}$$

$\sigma_{ref}$ is the reference stress calculated in accordance to Annex P of BS 7910. Alternatively, plastic limit loads $P_L$, may be derived from finite element analysis as discussed later.

# 3 GEOMETRY DEFINITION

## 3.1 Monopile Geometry

A flaw in an OWT monopile is selected as a case study for this paper. Monopile support structures represent approximately 90% of commissioned offshore wind structures [6]. OWT monopiles are fabricated by rolling and then welding thick structural steel plates in a longitudinal direction to produce "cans" which are then welded together circumferentially. The monopile has an outer radius, $r_o$ of 3m, inner radius, , $r_i$ of 2.9m and wall thickness, $t$ of 100mm in line with typical sizes of existing monopiles in various wind farms across Europe as reported in [7]. The length of the monopile is set as 40m which is the typical water depth of monopile foundation installations [8].

S355 steel is the most common material used in the fabrication of monopile support structure [9]. The material properties for S355 steel are as follows; the minimum yield strength, $\sigma_Y$ is taken as 335MPa, the tensile strength, $\sigma_u$ is taken as 470Mpa, the modulus of elasticity, E is 210Gpa [10]. The fracture toughness of S355 steel is taken as $38Mpa\sqrt{m}$ [11]. For the calculation of limit load, the onset of plasticity is set as the yield strength. This is in line with values recommended in ASME III Section NG-3224.1[12] for limit load calculations.

## 3.2 Crack Geometry

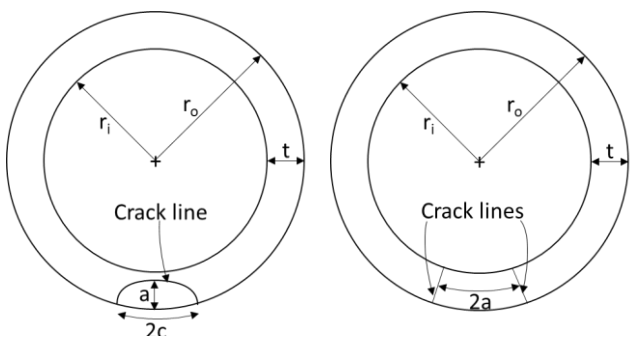


**(a) Semi Elliptical Surface Crack** **(b) Through Crack**

**Figure 3.1 – Crack Definition**

Cracks in monopiles typically start from a surface flaw situated at the weld/parent metal interface. The crack grows gradually as a semi-elliptical flaw until it penetrates the wall thickness (Figure 3.1a). At this point, it begins to propagate in the circumferential direction until two crack lines meet (Figure 3.1b).

The crack aspect ratio (crack depth/crack half length, a/c) is assumed as 0.4 based on recommendations in [13]. It is generally assumed that a semi-elliptical crack grows according to Paris law. Numerically, it is clear that for growth at all points along the crack line to obey the Paris relation, the crack growth at different points must be different to account for the variation in stress field triaxiality. Some research work such as [14] and [15] studied the evolution of aspect ratio and thus establish numerical solutions for the shape change of cracks during fatigue growth but the body of work in this field is light. For simplicity it is assumed that aspect ratio remains constant during crack growth.

# 4 FINITE ELEMENT MODELLING

The monopile is modelled in the finite element software package, ABAQUS [16]. The FE model is fixed at one end with a symmetry boundary condition (U3=UR1=UR2=0) in the Z direction (longitudinal axis of the cylinder). This allows a pure bending loading to develop in the monopile. The moment load is applied to a reference point coupled to free surface of the monopole. The axis of the moment load is oriented to cause crack opening under the applied load.

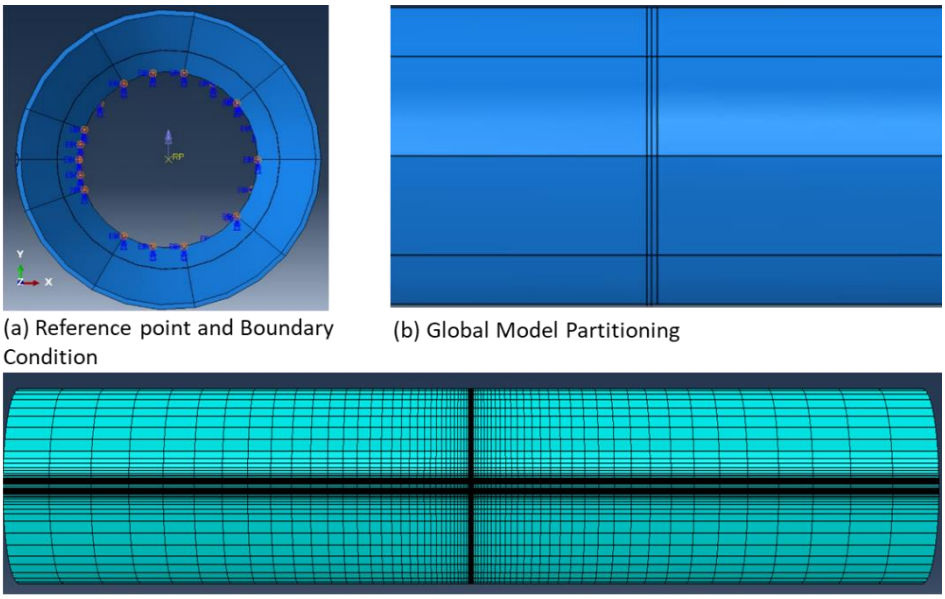

(a) Reference point and Boundary Condition

(b) Global Model Partitioning

(c) Side view of mesh

**Figure 4.1 – Finite Element Model**

The model is partitioned for ease of meshing and locating of the crack. The monopile is partitioned into nine sectors to facilitate a swept mesh. One sector is further partitioned to create a line through the centre of the intended cracked region (Figure 4.1a). The model is then partitioned at mid length to create a surface to locate the crack. Two further partitions above and below the partition at mid-length are created to form region surrounding the crack for finer meshing (Figure 4.1b). The rest of the model may then be coarsely meshed for computational efficiency (Figure 4.1c).

Detailed focused meshes are required around the crack tip for accurate contour integral evaluation. Abaqus integrates around the ring of element (contour) enclosing the crack tip to determine the stress intensity factor. Contour integrals are evaluated for multiple rings of elements surrounding the crack tip node. The first contour is formed from elements directly connected to the crack tip node. Each subsequent contour is created by offsetting one element away from the previous contour. There is some numerical variations in the values of SIF obtained from the integral evaluation of each contour. However, a large variation indicates a need for mesh refinement. There is no hard limit to the number of contours to be evaluated but at least 2 contours are required as the accuracy of the results from the first contour are heavily influenced by the crack tip.

## 4.1 Surface Crack Definition

A semi-elliptical partition is extruded through the length of the monopile. The edge created at the intersection of this extrusion and the mid-length partition is the crack line. Two additional semi-elliptical partitions are created, one towards the centre of the cylinder and the other towards the surface. These form the bounding region of the crack front in the thickness direction. The crack is modelled using the ABAQUS interaction module. The crack line is assigned, and the crack extension directions specified as q vectors normal to the crack plane at the different nodes along the crack

line. The reader is directed to the Abaqus manual [16] for further discussion on crack modelling within the software.

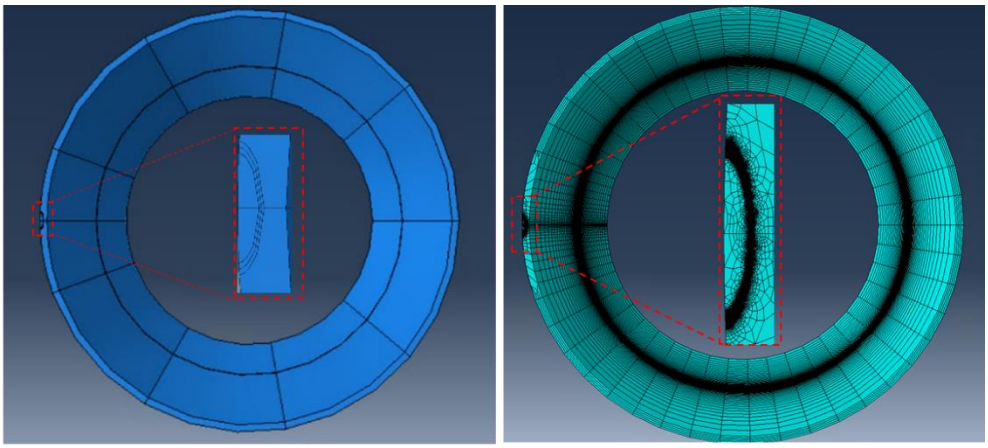

(a) Surface Crack Partitioning (b) Top View of Surface Crack Mesh

**Figure 4.2 – Surface Crack Definition**

## 4.2 Through-thickness Crack Definition

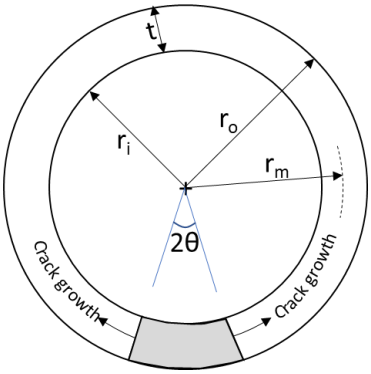


**Figure 4.3 - Through Thickness Crack Geometry**

A through thickness crack has two crack lines. One crack is advancing in the clockwise direction, the other in the anti-clockwise (Figure 4.3). To model the crack region in the FE software, six radial lines (3 per crack line) are extruded along the length of the monopile. One radial partition is the crack line whilst the remaining two partitions define the crack front region used in contour integral calculations (Figure 4.4a). The regions bounded within the raidal lines is finely meshed for accurate contour integral evaluation (Figure 4.4b). The position of the radial lines is dependent on the half angle (θ) of the crack being analysed.

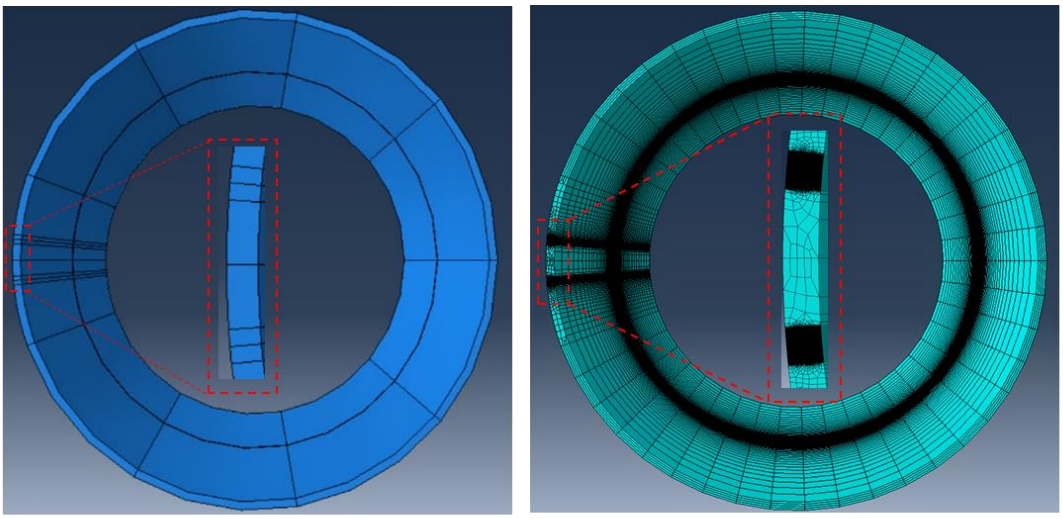

(a) Through-thickness Crack Partitioning (b) Top View of Through-thickness Crack Mesh

**Figure 4.4 – Through-thickness Crack Definition**

## 4.3 FE Loadcase

$K_r$ and $L_r$ values are extracted for the following surface crack depths: from 10 to 80mm in increments of 10mm and 80 – 95mm in increments of 5mm. $K_r$ and $L_r$ values are extracted for through cracks with half angles (θ) of 0.083rads, 0.1rads, 0.12rads, 0.14rad and 0.18rads. The analysis is terminated at a half angle of 0.18rads as the structure is expected to have crossed into the unsafe region of the FAD at this point. The starting half angle of 0.083rad is the half angle subtended by a surface crack with an aspect ratio (a/c) of 0.4 growing to through thickness of 100mm:

$$\theta = \frac{\left(t/\frac{a}{c}\right)}{r_o} = \frac{100/0.4}{3000} = 0.083rads \tag{4}$$

# 5 METHODOLOGY

## 5.1 Stress Intensity Factor – BS 7910

From various literature such as [17] and supported by Annex M.1 of BS 7910, the general form of the stress intensity factor for load applied normal to the crack plane (crack face) of an external surface crack oriented circumferentially growing in the thickness direction is described as:

$$K_I = (Y\sigma)\sqrt{\pi a} \tag{5}$$

$\sigma$ is the global applied stress;
$a$ is the crack depth;
$Y$ is the shape function which is dependent on the geometry of the cracked structure.

There are existing closed-form empirical equations for the shape function for a semi-elliptical surface crack in a finite plate such as those proposed by [18]. Annex M.1 of BS 7910 provides an expression for the calculation of shape factor for a structure subjected to primary stresses:

$$(Y\sigma)_p = Mf_w\{k_{tm}M_{km}M_mP_m + k_{tb}M_{kb}M_b[P_b + (k_m - 1)P_m]\} \tag{6}$$

$P_m$ and $P_b$ are the primary membrane and through-wall bending stresses respectively. $M, f_w, M_m, M_b$ are given for different types of flaws in different configurations in the standard. $M_{km}$ and $M_{kb}$ apply when a flaw is in a region of local stress concentration. $k_m$, $k_{tm}$, $k_{tb}$ account for stress concentration due to structural discontinuities or misalignment. For simplicity, $M_{km}$, $M_{kb}$ $k_m$, $k_{tm}$, $k_{tb}$are set to a value of 1 as stress concentrations and discontinuities are not included.

## 5.2 Reference Stress – BS 7910

For practical engineering applications, thin-walled assumption is adopted for pipes with ratio of diameter to thickness (D/t) greater than twenty. The monopile in the case study has a D/t=60 hence the reference stress is computed in accordance with the following BS 7910 clauses:

Clause P.10.4 for external surface flaw in thin walled pipe:

$$\sigma_{ref} = \frac{P_m\left[\pi(1 - a/t) + 2\left(\frac{a}{t}\right)\sin(c/r_o)\right]}{(1 - a/t)[\pi - (c/r_0)(a/t)]} + \frac{2P_b}{3(1 - \alpha")^2} \tag{7}$$

Clause P.10.1 for through thickness flaw in thin-walled pipe:

$$\sigma_{ref} = \frac{\pi(p_{m,a} + P_{m,p})}{\pi - \frac{a}{r_i} - 2arcsin\left(\frac{1}{2}sin\frac{a}{r_i}\right)} + \frac{\pi P_{m,b}(r_o^4 - r_i^4)}{\left[\pi - \frac{a}{r_i} - 2\frac{sin^2\left(\frac{a}{r_i}\right)}{\pi - \frac{a}{r_i}} - \frac{sin\left(\frac{2a}{r_i}\right)}{2}\right](4r_or_m^2t)} + \frac{2P_{b,l}}{3\left(1 - \frac{2a}{\pi r_i}\right)} \tag{8}$$

$P_{m,b}$, $P_{m,b}$, $P_{m,b}$ are membrane stresses due to external bending, axial loads and internal pressure respectively. $\alpha^{"} = \frac{a/t}{[1+(t/c)]}$ for $\pi r_o \geq c + t$ or $\frac{a/t}{(c/r_o)}$ for $\pi r_o < c + t$.

## 5.3 Stress Intensity Factor – FEA

Finite element simulation is performed on monopiles with various surface and through thickness cracks respectively to obtain the stress intensity factor (SIF) solution. The finite element model is meshed with linear hexagonal elements with reduced integration; C3D8R. Stress intensity factors are obtained in ABAQUS through the calculation of contour integrals. SIF results are obtained at four contours ahead of the crack line to bypass the variability of results obtained close to the crack line. Only SIF for mode I – opening mode is considered as the applied tensile stress is normal to the plane of the crack. Further information is provided in the Abaqus manual [16].

## 5.4 Limit Load - FEA

Limit load analysis is a well-established method for predicting margins against plastic collapse. The limit load is defined as the load that cause local yielding (ligament collapse) or causes net section yielding (global limit load). The limit load of a cracked structure may be determined from elastic-perfectly-plastic 3D finite element analyses.

To do this, an elastic-perfectly-plastic material curve is applied to the monopile with the onset of plasticity set as the yield strength. Incremental load is applied to the structure until the magnitude of the applied load cause global plastic collapse. This is signalled by the loss of static equilibrium due to excessive plasticity. The load applied at the final converged increment is the limit load [19]. It is noted that the limit load determined is applicable only to the specific geometry, include specific crack geometry and loading condition. Therefore, the analysis must be repeated for all crack geometries of interest.

To avoid problems associated with incompressibility, quadratic reduced integration elements within ABAQUS (element type: C3D20R) are used [20]. The reliability of the limit loads established from the finite element analysis is evidenced through comparison with theoretical solutions for uncracked pipes. A mesh study is also performed to verify that the solution has converged.

## 5.5 Structural Loads

OWT support structures are commonly designed according to loadcases specified in the IEC standard [21]. The list of Design Load Cases (DLCs) prescribed in the standard cover the various operating regimes of the wind turbine. A crack can experience three types of loading termed Mode I (opening mode), Mode II (shearing mode) and Mode III (tearing mode). The crack is assessed for Mode I loading which is typical for most fractures. For a crack subject to Mode I loading, the principal load is applied normal to the crack and tends to open the crack. Although the monopile is subject to various types of loads; compressive loads, shear forces and torsion, the primary Mode I crack opening loading is due to applied bending moment.

Morató [22] performed comprehensive aero-elastic analysis to determine the most onerous load case considering mudline overturning moment, blade root moments as metrics. The analysis shows that for a NREL 5MW wind turbine [23] based in a shallow water site in the Dutch North Sea [24], a combination typically assessed in research work, the maximum and minimum mudline overturning moment are 1.769E5 kNm and 1.230E5 kNm for the typical design loadcases. A bending moment load of 1.230E5 kNm induces a membrane stress of 45MPa in the outer fibres of the monopile and is considered for the assessment. For simplicity the through wall bending stress is ignored in the analysis and can be shown to be small for thin-walled structures

# 6 RESULTS AND DISCUSSION

## 6.1 BS7910 Results

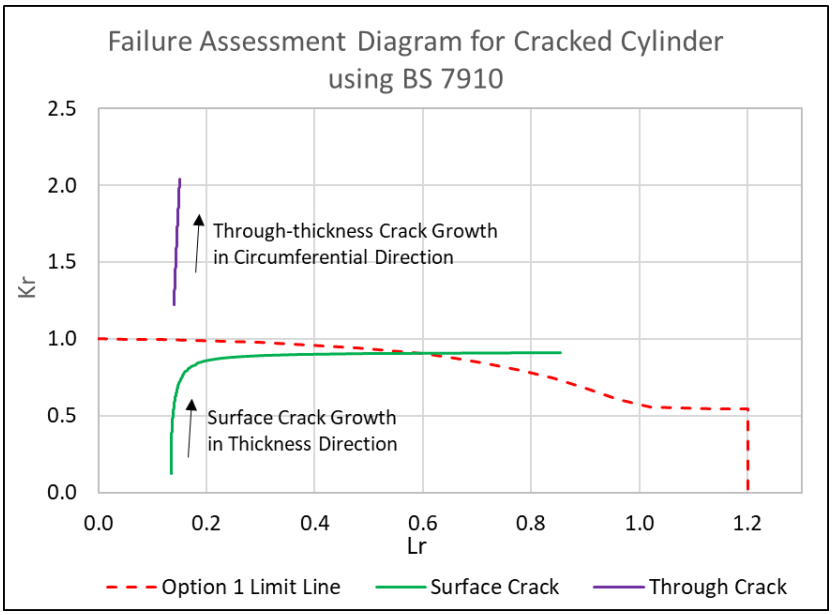


**Figure 6.1 – FAD for growing Circumferential Surface Crack and Through-thickness Crack**

The failure assessment diagram of a flaw growing from a surface crack until through thickness and for a through-thickness crack growing circumferentially is presented in Figure 6.1. The results show that for the applied stress, there is a surface crack depth which is unacceptable as it results in a combination of plastic collapse and brittle failure ratio that exceeds the FAD line.

However, examining the trends of the plastic collapse and brittle failure ratios reveals an anomaly. For the surface crack, the brittle failure ratio, $K_r$, is shown to increase monotonically with increasing surface crack depth. The plastic collapse ratio is initially insensitive to the crack depth. This is expected given the small size of the crack relative to the monopile, that is, there is sufficient intact ligament such that the monopile should not experience net section collapse due to loss of load bearing in the crack zone. However, the results show a rapid increase in the plastic collapse ratio as the crack depth to thickness ratio exceeds 80%.

The asymptotic trend is not present in the plastic collapse ratio for the through thickness crack. Whilst a discontinuity is expected in the jump from surface crack to through-thickness crack due to the additional ligament lost as the crack transitions from semi-elliptical to through thickness for the same depth to crack length ratio, it does not explain the rapid increase in the plastic collapse ratio for the semi elliptical crack.

It is clear that there is an issue with the calculation of plastic collapse ratio for a semi-elliptical crack for crack depths close to the value of the section thickness. A critical probing of the equation for reference stress suggests a purely numerical explanation for this behaviour. For a/c = 0.4, the maximum value of $c/r_0$ for this case study is 0.08. Therefore, as crack depth, a, approaches section thickness, t, the equation for reference stress for an external surface flaw may be simplified to:

$$\sigma_{ref} \approx P_m \left[1 + \frac{2c/r_0}{\pi}\left[\frac{a/t}{1-a/t}\right]\right] \tag{9}$$

The key component of equation (8) is $\frac{a/t}{1-a/t}$ which is plotted in Figure 6.2. The plot shows the exponential growth behaviour of the equation of values of a/t greater than 0.8. Figure 6.2 indicates

an inherent flaw in the calculation of reference stress for cases where the crack has penetrated more than 80% of the monopile thickness.

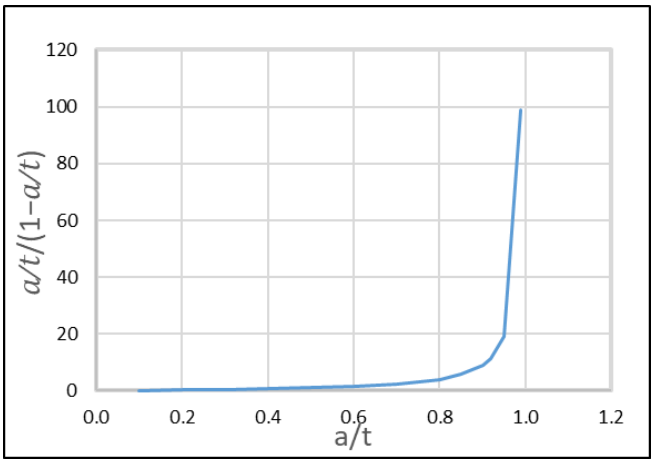


**Figure 6.2 – Plot of $\frac{a/t}{1-a/t}$ against a/t**

This behaviour is of less concern for cylinders where there is little margin between 80 – 100% of thickness. However, for monopiles, this range may cover a value of 20mm or greater. Crack growth as a large flaw, e.g. when the crack depth exceeds half the thickness of the monopile thickness, forms a significant part of the total life.

The invalidity of the reference stress equation for surface crack depths greater than 80% of section thickness is not explicitly stated in clause P.10.4 of BS 7910. The only specified limit of 80% is on the ratio of crack half-length to the pipe radius, c/ $r_o$. For this case study, even considering flaw that is almost through the thickness and a low value of a/c=0.1, c/ $r_o$ is approximately 33%.

Taking the findings together, it is possible that a monopile with a circumferential surface flaw may be identified as close to plastic collapse failure when there may still be significant residual life for a situation where the ratio of crack depth to section thickness, a/t is greater than 80%.

## 6.2 FEA Results

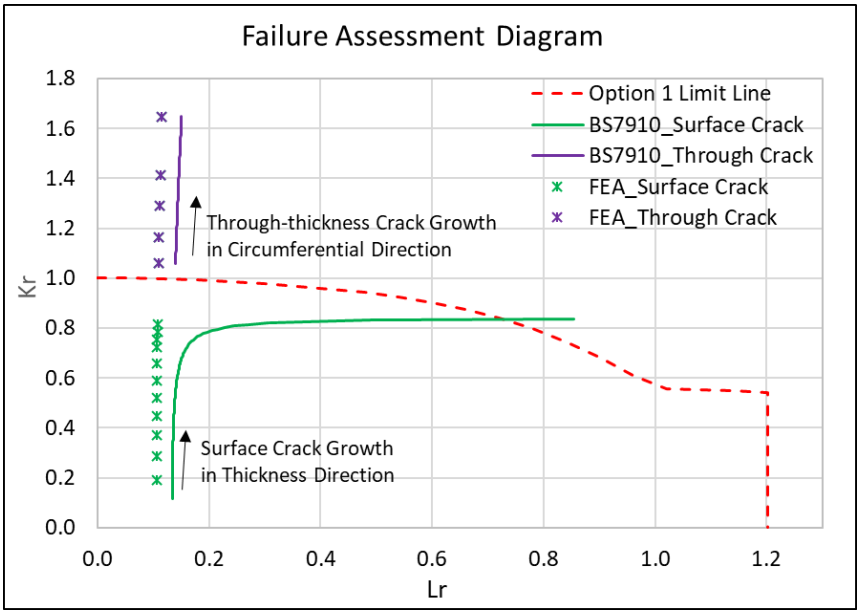


**Figure 6.3 – FAD for Circumferential Surface Crack and Through-thickness Crack**

A plot of the fracture and load ratios obtained from the FE analyses against the values calculated for the same geometry using the equations prescribed in the industrial standard BS 7910 [3] is presented in Figure 6.3. The fracture ratio, $K_r$ and the load ratio, $L_r$ are calculated based on stress intensity factor and limit loads obtained from FE analyses of various cracked geometry. The findings from the comparison presented as follows:

### 6.2.1 Load Ratio Comparison

Figure 6.3 shows agreement between both FE analysis and BS 7910 that there is little impact initially on the load ratio as the crack grows. This is expected as there is significant connected ligament in the rest of the structure such that the crack has little impact on the static load bearing capacity of the structure. This is in line with experimental observations by [25].

Figure 6.3 also shows that the load ratio obtained by FE analysis is slightly smaller than the value predicted by BS 7910. This is unsurprising as one would expect the results obtained from the application of a general code to be conservative compared to a bespoke analysis due to the necessary assumptions involved in collating the equations for BS 7910. However, the major difference in the FE results and BS 7910 arise as the surface crack approached through thickness. The FE results do not exhibit the asymptotic behaviour as shown in the BS 7910 calculations. Figure 6.3shows that the FE results proceed with the same trend as the surface crack transitions to a through thickness crack.

### 6.2.2 Fracture Ratio Comparison

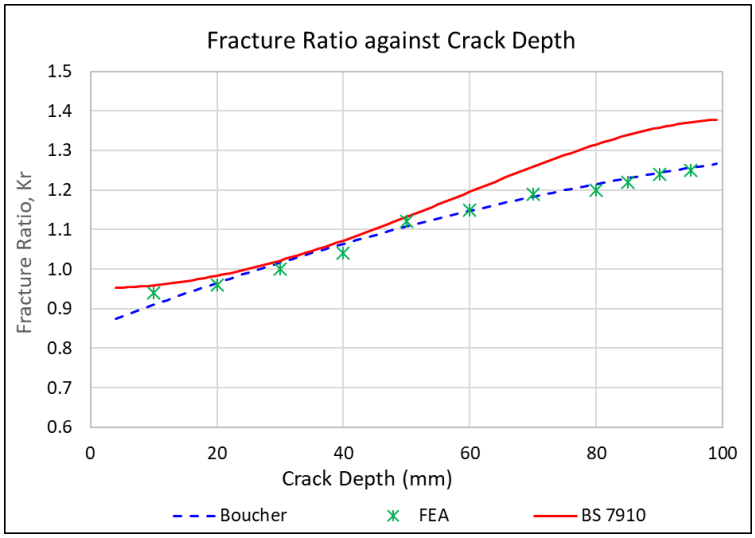


**Figure 6.4 – Fracture Ratio against Crack Depth**

The SIF solution in BS 7910 for a circumferential external surface crack in a cylinder is based on the flat plate solution underpinned by the empirical stress intensity factor equation for a semi-elliptical surface crack in a finite plate proposed by J.C. Newman and I.S. Raju [18] and [26].

It is shown in recent work by Bocher [8] that for pipes with large radius/thickness ratios as is common in monopiles, these solutions provide inaccurate estimation of the shape function. The results presented in Figure 6.4 show that there is alignment between the current work and the results presented by Bocher [8].

Figure 6.3 shows a minor discontinuity between the $K_r$ value for a surface crack depth of 95mm and a through crack with a half angle of 0.083rads. This is due to the additional ligament lost as the crack transitions from semi-elliptical to through thickness for the same depth to crack length ratio.

# 7 CONCLUSION AND FUTURE WORK

This paper presents an assessment of the fitness for purpose of an offshore wind turbine monopile with a known semi-elliptical surface flaw in accordance with the procedure outlined in the industry standard, BS 7910 and comparison with results obtained from finite element analysis.

The results presented in this paper highlight the issues with the calculation of the load ratio, $L_r$ using the methodology outlined in BS 7910 for cracks with depths greater than 80% of the monopile thickness. $L_r$ values for deep cracks calculated from BS 7910 exhibit an asymptotic behaviour as the crack depth nears through thickness.

The load ratio values obtained from detailed 3D FE limit analysis using elastic-perfectly-plastic material behaviour show that the asymptotic behaviour predicted by BS 7910 as the flaw transitions from deep crack to through-thickness crack is not present. Furthermore, the fracture ratio, $K_r$, predicted by BS 7910 is an over-estimation for the typical dimensions of offshore monopiles. This confirms the findings by other researchers such as Bocher [8].

Taken together, the findings suggest that it is possible that a structure with a deep flaw may be erroneously identified as unacceptable based on BS 7910 when there may still be a non-trivial amount of residual life.

There are additional issues with the use of BS 7910 for offshore monopiles such as the lack of sufficient library of shape function (Y) solutions for cylinders with large radius to thickness ratios. There is also a lack of information on the evolution of crack shape for cylinders under bending. It is assumed that initially elliptical flaws remain elliptical as they grow and that the crack aspect ratio remains the same. However, it may be important to account for different growth rates at different points along the crack. Further research is required to address these issues to allow BS 7910 to be used confidently to assessing the acceptability of flaws in offshore wind turbine monopiles.

# 8 ACKNOWLEDGEMENT

This research is supported through the Centre for Doctoral Training (CDT) in Renewable Energy and Marine Structure (REMS) at the University of Strathclyde. REMS is an Engineering and Physical Sciences Research Council (EPSRC) funded CDT. Finite element analysis results were obtained using the ARCHIE-WeST High Performance Computer (www.archie-west.ac.uk) based at the University of Strathclyde.

# 9 REFERENCES

[1] L. Ziegler, E. Gonzalez, T. Rubert, U. Smolka, and J. J. Melero, "Lifetime extension of onshore wind turbines: A review covering Germany, Spain, Denmark, and the UK," *Renewable and Sustainable Energy Reviews,* vol. 82, pp. 1261-1271, 2018.

[2] G. L. DNV, "DNVGL-ST-0126: Support structures for wind turbines," *Oslo, Norway: DNV,* 2016.

[3] B. Standard, "BS 7910: 2013+ A1: 2015 Guide to methods for assessing the acceptability of flaws in metallic structures," *London, UK: BSI Stand Publ,* 2015.

[4] A. P. I. API, "579-1/ASME FFS-1: Fitness-for-service," *The American Society of Mechanical Engineers,* 2007.

[5] I. Hadley, "BS 7910: 2013 in brief," *International Journal of Pressure Vessels and Piping,* vol. 165, pp. 263-269, 2018.

[6] F. P. Brennan, "A framework for variable amplitude corrosion fatigue materials tests for offshore wind steel support structures," *Fatigue & Fracture of Engineering Materials & Structures,* vol. 37, no. 7, pp. 717-721, 2014.

[7] L. Arany, S. Bhattacharya, J. Macdonald, and S. J. Hogan, "Design of monopiles for offshore wind turbines in 10 steps," *Soil Dynamics and Earthquake Engineering,* vol. 92, pp. 126-152, 2017.

[8] M. Bocher, A. Mehmanparast, J. Braithwaite, and M. Shafiee, "New shape function solutions for fracture mechanics analysis of offshore wind turbine monopile foundations," *Ocean Engineering,* vol. 160, pp. 264-275, 2018.

[9] V. Igwemezie, A. Mehmanparast, and A. Kolios, "Materials selection for XL wind turbine support structures: A corrosion-fatigue perspective," *Marine Structures,* vol. 61, pp. 381-397, 2018.

[10] En, "Eurocode 3: Design of steel structures: General rules and rules for buildings," ed: CEN, European Committee for Standardization Brussels, 2005.

[11] F. Bozkurt and E. Schmidová, "Fracture Toughness Evaluation of S355 Steel Using Circumferentially Notched Round Bars," *Periodica Polytechnica Transportation Engineering,* vol. 47, no. 2, pp. 91-95, 2019.

[12] *Section III: Rules for construction of nuclear facility components*, ASME, New York, 2015.

[13] DNV, "DNVGL-RP-C210: Probabilistic Methods for Planning of Inspection for Fatigue Cracks in Offshore Structures," *Det Norske Veritas & Germanischer Lloyd SE: Oslo, Norway,* 2015.

[14] S.-X. Wu, "Shape change of surface crack during fatigue growth," *Engineering Fracture Mechanics,* vol. 22, no. 5, pp. 897-913, 1985.

[15] J. Toribio, J.-C. Matos, and B. González, "Aspect ratio evolution in embedded, surface, and corner cracks in finite-thickness plates under tensile fatigue loading," *Applied Sciences,* vol. 7, no. 7, p. 746, 2017.

[16] *User Manual*. (2016). SIMULIA.

[17] T. L. Anderson, "Fracture mechanics-fundamentals and applications," *NASA STI/Recon Technical Report A,* vol. 92, 1991.

[18] J. C. Newman Jr and I. S. Raju, "Analyses of surface cracks in finite plates under tension or bending loads," NATIONAL AERONAUTICS AND SPACE ADMINISTRATION HAMPTON VA LANGLEY RESEARCH …, 1979.

[19] M. R. Booth, "Applying Finite Element Based Limit Load Analysis Methods to Structures Under Dynamic Loads," 2014 2014, vol. 45981: American Society of Mechanical Engineers, p. V001T01A005.

[20] Y.-J. Kim, D.-J. Shim, K. Nikbin, Y.-J. Kim, S.-S. Hwang, and J.-S. Kim, "Finite element based plastic limit loads for cylinders with part-through surface cracks under combined loading," *International Journal of Pressure Vessels and Piping,* vol. 80, no. 7-8, pp. 527-540, 2003.

[21] I. E. C. Iec, "61400-3, Wind Turbines-Part 3: Design Requirements for Offshore Wind Turbines," *International Electrotechnical Commission, Geneva,* 2009.

[22] A. Morató, S. Sriramula, N. Krishnan, and J. Nichols, "Ultimate loads and response analysis of a monopile supported offshore wind turbine using fully coupled simulation," *Renewable Energy,* vol. 101, pp. 126-143, 2017.

[23] J. Jonkman, S. Butterfield, W. Musial, and G. Scott, "Definition of a 5-MW reference wind turbine for offshore system development," National Renewable Energy Lab.(NREL), Golden, CO (United States), 2009.

[24] T. Fischer, W. E. De Vries, and B. Schmidt, "UpWind design basis (WP4: Offshore foundations and support structures)," 2010.

[25] F. M. Burdekin, B. Talei-Faz, F. P. Brennan, and W. D. Dover, "Experimental validation of the ultimate strength of brace members with circumferential cracks," *OFFSHORE TECHNOLOGY REPORT-HEALTH AND SAFETY EXECUTIVE OTO,* 2002.

[26] J. C. Newman and I. S. Raju, "Stress-intensity factor equations for cracks in three-dimensional finite bodies," 1983 1983: ASTM International.